Barocaloric effect in metamagnetic shape memory alloys.

Lluís Mañosa [*,1], Enric Stern-Taulats [1], Antoni Planes [1], Pol Lloveras [2], Maria Barrio [2], Josep-Lluís Tamarit [2], Baris Emre [3], Suheyla Yüce [4], Simone Fabbrici [5,6], Franca Albertini [6]

[1] Departament d'Estructura i Constituents de la Matèria. Facultat de Física. Universitat de Barcelona. 08028 Barcelona. Catalonia.
[2] Departament de Física i Enginyeria Nuclear. ETSEIB. Universitat Politècnica de Catalunya. 08028 Barcelona. Catalonia.
[3] Department of Engineering Physics, Faculty of Engineering, Ankara University. 06100 Besevler, Ankara. Turkey
[4] Department of Physics, Science and Literature Faculty, Ondokuz Mayis University, Kurupelit 55139, Samsun, Turkey.
[5] MIST E-R Laboratory, Via Gobetti 101, 40129 Bologna, Italy.
[6] IMEM-CNR, Parco Area delle Science, 37/A, 43100 Parma, Italy.

Received XXXX, revised XXXX, accepted XXXX
Published online XXXX

Key words: Barocaloric,Shape Memory, Metamagnetic, Pressure.

* Corresponding author: e-mail lluis@ecm.ub.edu,

We report on calorimetric measurements under hydrostatic pressure in a series of composition related metamagnetic shape memory alloys. We show that metamagnetic shape memory alloys exhibit a barocaloric effect whose magnitude compares well to the magnetocaloric effect exibited by this kind of alloys. While in metamagnetic alloys the magnetocaloric effect is inverse, the barocaloric effect has been found to be conventional. The values obtained for the pressure-induced entropy changes at moderate pressures are in the range of those reported for giant caloric materials.

Copyright line will be provided by the publisher

1 Introduction Magnetic shape memory alloys are a class of materials exhibiting large reversible deformations under the application and removal of a magnetic field [1]. Such a unique property is associated with a strong coupling between magnetism and structure at the martensitic transition undergone by these alloys between a high temperature cubic phase (austenite) and a low temperature denser phase (martensite). The magneto-structural coupling can take place at several length-scales [2]. At a microscopic scale, the different crystallographic structure between martensite and austenite leads to a different magnetization of the two phases. In this case, application of magnetic field enhances the stability of the phase with the highest magnetization and the structural transition can be induced by application of magnetic field. This behaviour corresponds to the magnetic superelasticity [3,4]. Coupling at a mesoscopic scale refers to the coupling between martensitic variants and magnetic domains. In that case, the stronger magnetocrystalline anisotropy of the martensitic phase promotes rotation of the martensitic variants under the application of a magnetic field thus leading to the so-called magnetic shape memory [5]. In addition to magnetic shape memory and magnetic superelasticity these alloys have been reported to exhibit a number of properties such as magnetocaloric (conventional and inverse) [6–8] and elastocaloric [9] effects, magnetoresistance [10], exchange biass [11] and kinetic arrest [12]. Also spin-glass [13] and strain-glass [14] behaviour has been reported on several of these compounds.

In shape memory alloys, the martensitic transition usually takes place with a negligible volume change. However in magnetic alloys the balance between magnetic and structural free energies can lead to differences in the volume of the unit cell of the austenitic and martensitic phases [15, 16]. In that case, the martensitic transition will be sensitive to applied hydrostatic pressure as has been shown to be the case in Ni-Mn-In alloys [17]. A pressure-induced magneto-structural phase transition opens-up the possibility for the alloy to exhibit a barocaloric effect associated with the latent heat of the phase transition. A giant barocaloric effect was recently reported for a Ni-Mn-In magnetic shape memory alloy [18] and later, other giant magnetocaloric materials were also shown to exhibit large barocaloric effects [19, 20].

Copyright line will be provided by the publisher

In the present paper we report on the barocaloric effect in a series of composition-related metamagnetic shape memory alloys (Co and In-doped Ni-Mn-Ga). The paper is organized as follows: experimental details are provided in section 2, while the experimental results are presented in section 3. A discussion of the obtained results is given in section 4, and section 5 provides a summary and the main conclusions of the work.

2 Experimental Details The samples were prepared by arc-melting the stoichiometric quantities of the elements. To prevent oxydation an inert atmosphere in the furnace chamber was established by the repeated inlet of high purity Ar gas followed by vacuum cycles; in order to strip the residual oxygen from the chamber, a prolonged melting of a Ti getter occurred just before the melting of the samples. In order to improve homogeneity, the samples were remelted four times, while the total weight loss was kept below 2%. The samples were annealed at 800 ^{o}C for 72h in high purity Argon. The compositions (in at%) of the prepared samples, measured by EDX were $Ni_{43.3}Co_{7.4}Mn_{30.8}Ga_{18.5}$ (sample In0); $Ni_{42.47}Co_{8.87}Mn_{31.67}Ga_{14.98}In_{2.01}$ (sample In20) and $Ni_{42.2}Co_{8.4}Mn_{32.4}Ga_{15}In_{2.1}$ (sample In21). Sample In20 is obtained from the same ingot than the sample previously investigated by calorimetry under magnetic field (labelled In2 in ref. [21]). From the ingots, samples for magnetic measurements and conventional DSC (typical mass $\sim$ 0.14 - 0.16 g), and for calorimetry under pressure (typical mass $\sim$ 1.7 - 1.8 g) were cut using a low-speed diamond saw. Crushed powders prepared for X-ray measurements were annealed before the measurements to improve crystallinity.

X-ray diffraction patterns were collected by using a Thermo ARL X-ftra diffractometer equipped with a solid-state Si(Li) Peltier detector and an environmental chamber which allows to perform measurements in the range 100-600K.

Thermomagnetic analysis (TMA), was used to determine the temperature dependence of the ac susceptibility in an applied field of a few Oe. Conventional differential scanning calorimetry (DSC) was conducted using a Q-2000 calorimeter from TA Instruments. Hydrostatic pressure calorimetry was carried out in a custom-built calorimeter described in ref. [18]. In that device the thermal signal was measured by a chromel-alumel thermocouple embedded into the sample. From calorimetric curves at selected values of the hydrostatic pressure, the entropy change (referenced to a given state at T_0 above the phase transition) is computed as described in [19].

3 Results Examples for the X-ray diffraction patterns collected at selected temperatures are shown in Figure 1 (left panels) for samples In20 and In21. For the sake of clarity, data collected during cooling runs are not displayed in the Figure. The selected range displayed in Fig. 1 highlights the onset of the austenitic phase and the concurrent

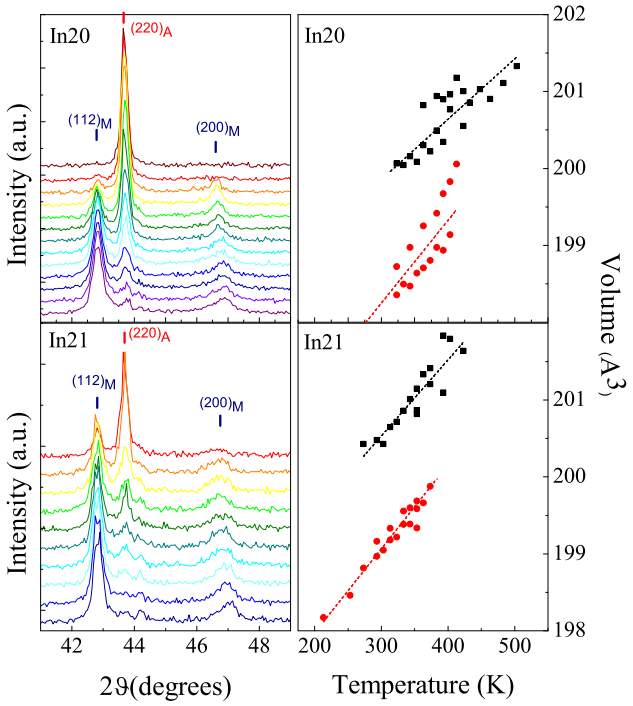

Figure 1 Left panels: Xray diffraction patterns at selected values of temperature. For sample In20 (top panel) temperatures from top to bottom are: 448,423,413,403,393,383,373,363,353,343,333,323,313K. For sample In21 (bottom panel) temperatures from top to bottom are: 373,353,343,333,323,313,303,293,273,253,213K. Right panels: temperature dependence of the unit cell volume in the austenitic (squares) and martensitic (circles) phases. Lines are linear fits to the data.

fading of the martensitic reflections while the austenitic peak steadily grows on heating. The austenitic phase has been found to be cubic, and the martensitic phase, tetragonal non modulated for the two samples. Lattice parameters for the different structures have been refined for each temperature. The values obtained at the transition temperatures are: a_A= 5.855 $\pm$ 0.003 Å ; a_M= 3.893 $\pm$ 0.005 Å and c_M= 6.57 $\pm$ 0.01 Å for the austenitic and martensitic phases of sample In20, and a_A= 5.859 $\pm$ 0.005 Å ; a_M= 3.900 $\pm$ 0.005 Å and c_M= 6.56 $\pm$ 0.01 Å for the austenitic and martensitic phases of sample In21. From the refined lattice parameters, the crystal volume of the two phases is obtained as a function of temperature. Results are shown in Figure 1 (right panels) for samples In20 and In21. The thermal expansion of the two phases is different, and the relative volume change shows a non-negligible drift with temperature. At the transition temperature the relative volume change is $\Delta v/v$ = 0.7 $\pm$ 0.2 % for In20 and $\Delta v/v$ = 0.7 $\pm$ 0.3 % for In21.

Copyright line will be provided by the publisher

Table 1 Transition temperatures, T_c,M_s,M_f,A_s,A_f; transition entropy change ΔS_t; pressure dependence of the transition (peak) temperature dT/dp and transition volume change Δv.

Sample	T_c(K)	M_s(K)	M_f(K)	A_s(K)	A_f(K)	ΔS_t(J/kg K)	dT^c/dp (K/kbar)	dT^h/dp (K/kbar)	Δv (10^{-7}m^3/kg)
In0	440	405	387	403	419	16.4	3.2	2.0	4 ± 1
In20	435	423	398	416	430	22.8	3.2	2.1	6 ± 1
In21	430	390	367	382	399	21.2	2.7	2.7	6 ± 1

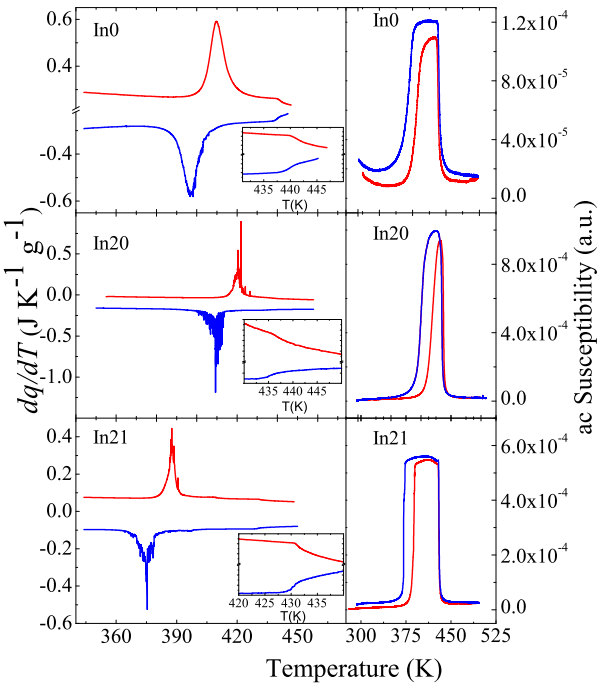

Figure 2 Left panels: differential scanning calorimetry curves for the three studied samples. On each panel bottom curves correspond to cooling runs and upper curves, to heating runs. The inserts show enlarged views of the calorimetric curves to illustrate the feature associated with the Curie point. Right panels: temperature difference of the ac magnetic susceptibility.

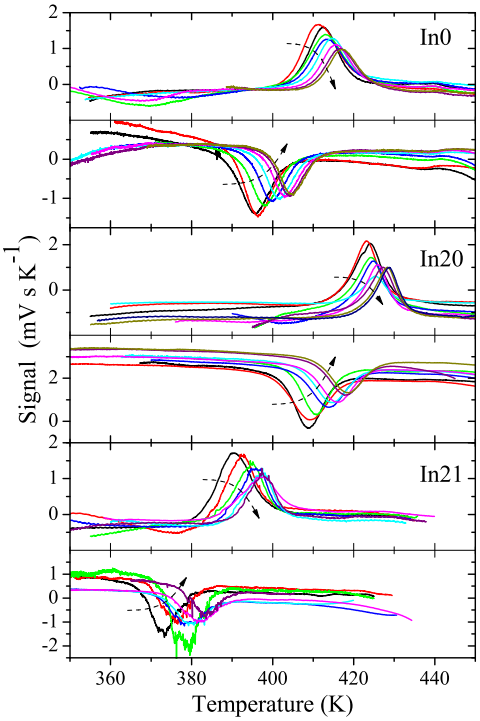

Figure 3 Calorimetric curves at selected values of the hydrostatic pressure. On each panel bottom curves correspond to cooling runs and upper curves, to heating runs. Dashed arrows indicate increasing pressure. Curves correspond to pressures of 0.5, 1.0, 1.5, 2.0, 2.5 and 2.8 kbar for sample In0; 0.5, 1.0, 1.2, 1.5, 2.0, 2.5, and 2.7 kbar for sample In20; and 0.5, 1.0, 1.5, 2.0, and 2.5 kbar for sample In21.

Figure 2 (left panels) shows heating and cooling DSC curves for the three studied alloys. A tiny feature at high temperatures (illustrated in the inserts) corresponds to the Curie point of the cubic phase, and large and broad exothermal and endothermal peaks correspond, respectively, to the forward and reverse martensitic transitions. The jerky character of the curves reflects the avalanche behaviour kinetics of the martensitic transition [22]. The values for the characteristic temperatures austenite start (A_s), austenite finish (A_f), martensite start (M_s), martensite finish (M_f) and Curie point (T_c) are listed in Table 1. Numerical integration of DSC curves renders the transition entropy values ΔS_t. Within experimental error, no significant differences have been found between cooling and heating data, and average values are listed in Table 1.

The temperature dependence of the ac susceptibility is also shown in Figure 2 (right panels). Upon cooling, there is a significant increase in the susceptibility at the Curie point, and a marked hysteretic decrease occurs at the martensitic transition. The transition temperatures determined from TMA curves coincide with those obained from the calorimetric curves.

Representative examples of the thermal curves obtained during heating and cooling at selected values of hydrostatic pressure are shown in Figure 3 for the three studied samples. The exothermal and endothermal peaks associated with the martensitic transformation are clearly visible. Both, forward and reverse transitions shift to high temperatures as pressure is increased. This behaviour is

Copyright line will be provided by the publisher

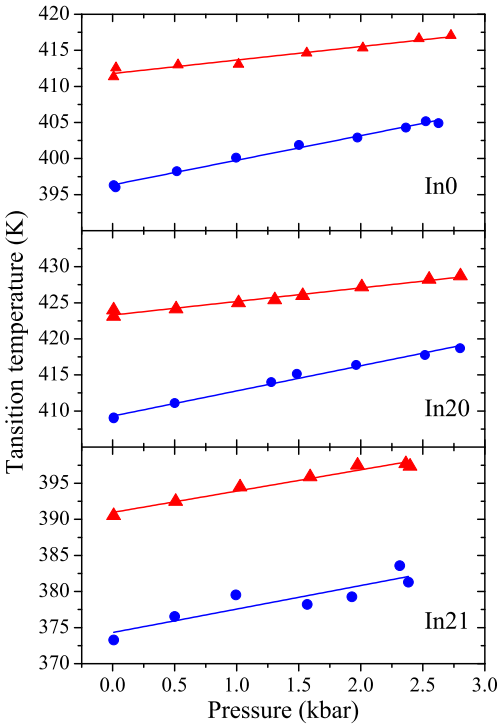

Figure 4 Transition temperatures for the forward (blue circles) and reverse (red triangles) transitions as a function of hydrostatic pressure.

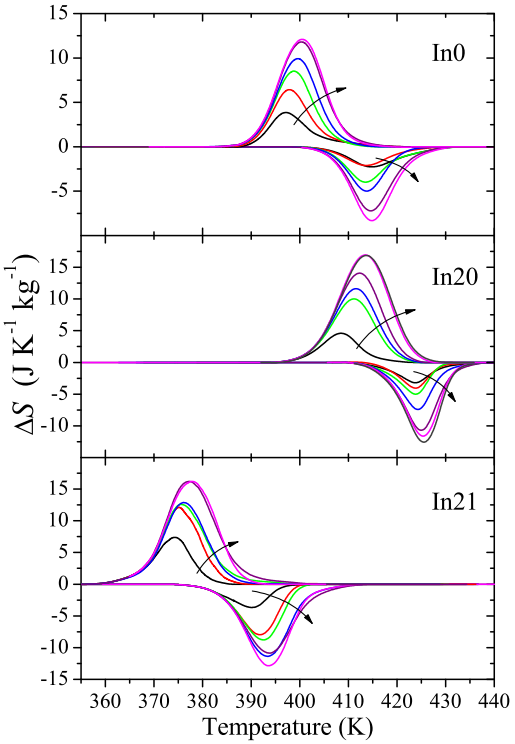

Figure 5 Isothermal pressure-induced entropy change (barocaloric effect) as a function of temperature. On each panel upper curves correspond to data obtained from cooling runs and lower curves, to data obtained from heating runs. The arrow indicates increasing pressure. Curves correspond to pressures of 0.5, 1.0, 1.5, 2.0, 2.5 and 2.8 kbar for sample In0; 0.5, 1.0, 1.2, 1.5, 2.0, 2.5, and 2.7 kbar for sample In20; and 0.5, 1.0, 1.5, 2.0, and 2.5 kbar for sample In21.

consistent with the lower value of the unit cell volume of the martensitic phase (Fig. 1), which enhances its stability by pressure. The values for the peak temperatures are depicted in Figure 4 as a function of the applied pressure. The increase is found to be linear, and values for dT/dp are listed in Table 1. The shift for the forward transition with pressure is slightly larger than that of the reverse transition (except for sample In21) which results in a reduction of the thermal hysteresis of the transition with increasing pressure.

The pressure-induced entropy change (barocaloric effect), ΔS, can be computed from the thermal curves in Figure 3, following the procedure described in ref. [19]. Results are shown in Figure 5. The barocaloric effect found for metamagnetic shape memory alloys is conventional, i.e., application of pressure causes a reduction in the alloy's entropy. For convenience, values computed from heating runs are plotted as negative data while values computed from cooling runs are plotted as positive data. As will be discussed later such a representation enables to elucidate the reversibility of the barocaloric effect [21]. The pressure-induced entropy change increases with increasing pressure, as illustrated in Figure 6 (left panel) which shows the maximum pressure-induced entropy values ΔS_{max} as a function of pressure.

We have computed the Refrigerating Cooling Power (RCP) as $RCP = \Delta S_{max} \times \delta T_{FWHM}$ [23]. Results for cooling and heating runs are shown in Figure 6 (right panel) as a function of pressure. The increase in RCP with increasing pressure is a consequence of the increase in ΔS_{max} and the broadening of the ΔS vs T peak (Figure 5) resulting from the shift in the martensitic transition to higher temperatures with increasing pressure. The RCP values found for the barocaloric effect in metamagnetic alloys compare well to those reported for magnetocaloric materials at moderate magnetic fields [24].

4 Discussion Metamagnetic shape memory alloys undergo a martensitic transition which involves a change in the magnetic properties as well as a change in the volume of the unit cell. These changes enable the transition to be driven both by application of a magnetic field and hydrostatic pressure which gives rise, respectively, to the magnetocaloric and barocaloric effects in these alloys. The large values for the magnetic field-induced and pressure-induced entropy changes are associated with the latent heat

Copyright line will be provided by the publisher

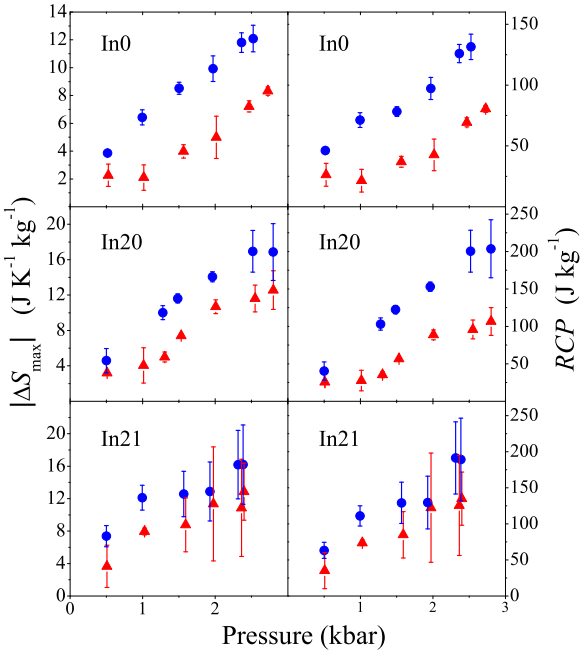

Figure 6 Left panels: Absolute value for the maximum pressure-induced entropy change as a function of pressure. Right panels: Refrigerating Cooling Power as a function of pressure. Blue circles correspond to data from cooling runs and red triangles, to data from heating runs.

of the transition. The lower magnetization of the martensitic phase gives rise to an inverse magnetocaloric effect (increase in entropy by application of a magnetic field), in agreement with the shift of the transition temperatures to lower values as magnetic field is increased. By contrast, the barocaloric effect has been found to be conventional (decrease in entropy by application of pressure), reflecting the lower volume of the martensitic unit cell. Accordingly, the transition shifts to higher temperatures with increasing pressure. The volume change at the martensitic transition can be obtained by using the Clausius-Clapeyron equation: $\Delta v = \Delta S_t \; dT/dp$. Within experimental errors ΔS_t has been found to be independent of pressure for the studied range of pressures. Hence, the good linearity exhibited by the transition temperature vs. pressure (see Fig. 4) indicates that the volume change at the transition does not depend on pressure. The computed values for Δv are listed in Table 1. For samples In20 and In21 they correspond to relative changes of $\frac{\Delta v}{v} = 0.5 \pm 0.1$ % (for the two samples), where the unit cell volume for the two samples is taken as v=1.25 10^{-4} m^3/kg, computed from x-ray data. Although values in Table 1 are slightly lower than those from x-ray, there is a quite good agreement between the two set of data taking into account the uncertainties associated with the two methods.

The values for ΔS_{max} found in present metamagnetic alloys are comparable to those reported for Gd-Si-Ge [20] and slightly lower than those for Ni-Mn-In alloys [18]. They are larger than the values reported for La-Fe-Si magnetocaloric materials [19]. The upper bound for the pressure-induced entropy change is given by the transition entropy change ΔS_t. From Fig. 6 it is apparent that for the three alloys ΔS_{max} does not reach the upper bound value for the range of studied pressures. This is a consequence that the pressure is not large enough to promote the transformation of the full sample.

The reversibility in a caloric effect is provided by the reproducibility in the ΔS (or ΔT) values for a cycling variation of the external field. The calorimeter used in our experiments operates at constant pressure and sweeping temperature but does not enable to isothermally sweep the applied pressure. However a recent calorimetric study of the magnetocaloric effect under isofield and isothermal conditions has shown that the reproducibility of the caloric effect can also be assessed from isofield data recorded during heating and cooling runs [21]. For a conventional caloric effect (as the barocaloric effect found here) the temperature region where the effect is expected to be reproducible is bounded by the martensitic start transition under applied pressure and the austenite start transition at atmospheric pressure. A graphical approach is provided by the temperature region where the ΔS vs T curves recorded on heating and cooling overlap. Inspection of Figure 5 suggests a poor reproducibility for the barocaloric effect in the studied metamagnetic alloys. Such a lack of reproducibility must be ascribed to a relatively large hysteresis of the transition $\sim 15K$ and a moderate pressure dependence of the transition temperatures. Taking into account the pressure dependence of the transition temperatures and the values for the thermal hysteresis we can estimate that pressures of ~ 8 kbar would be necessary to obtain a reversible barocaloric effect.

5 Summary and Conclusion. Metamagnetic shape memory alloys exhibit magnetocaloric and barocaloric effects under the application (or removal) of magnetic field and hydrostatic pressure, respectively. While the magnetocaloric effect is inverse, the barocaloric effect is conventional. The two effects have the same physical origin: the first-order martensitic transition which involves a significant latent heat, that can be induced either by magnetic field or by hydrostatic pressure.

The values obtained for the entropy changes at the barocaloric effect at moderate pressures compare well to those for the magnetocaloric effect [21], and they are in the range of the values reported for materials exhibiting giant caloric effects [25].

Although the relatively large thermal hysteresis compromises the reproducibility of the barocaloric effect, a good reproducibility for the magnetocaloric effect has recently been reported [21], associated with the strong sen-

Copyright line will be provided by the publisher

sitivity of the martensitic transition to the magnetic field. Moreover, the opposite behaviour of the transition temperatures with magnetic field and pressure suggests that the reproducibility could be enhanced (increased temperature region and entropy values) either by tuning the magnetocaloric effect by hydrostatic pressure or by tuning the barocaloric effect by a magnetic field.

Acknowledgements Financial support is acknowledged to CICyT (Spain) Projects No. MAT2010-15114, and FIS2011-24439 and AGAUR (Catalonia) Project 2009SGR-1251. E. Stern-Taulats acknowledges a fellowship from AGAUR (Catalonia).

References

[1] M. Acet, L. Mañosa, and A. Planes, *Handbook of Magnetic Materials*, **19**, 231 (2011).
[2] A. Planes, L. Mañosa, and M. Acet, J. Phys.:Condens. Matter. **21**, 23201 (2009).
[3] T. Krenke, E. Duman, M. Acet, E.F. Wassermann, X. Moya, L. Mañosa, A. Planes, E. Suard, and B. Ouladdiaf, Phys. Rev. B **75**, 104414 (2007).
[4] R. Kainuma, Y. Imano, W. Ito, Y. Sutou, H. Morito, S. Okamoto, O. Kitakami, K. Oikawa, A. Fujita, T. Kanomata, and K. Ishida, Nature **439**, 957 (2006).
[5] K. Ullakko, J.K. Huang, C. Kantner, R.C. O'Handley, and V.V. Kokorin, Appl. Phys. Lett. **69**, 1966 (1996).
[6] F.X. Hu, B.G. Shen, and J.R. Sun, Appl. Phys. Lett. **76**, 3460 (2000).
[7] T. Krenke, E. Duman, M. Acet, E.F. Wassermann X. Moya, L. Mañosa, and A. Planes, Nature Mater. **4**, 450 (2005).
[8] L. Pareti, M. Solzi, F. Albertini, and A. Paoluzi, Eur. Phys. J. B **32**, 303 (2003).
[9] P.O. Castillo-Villa, D.E. Soto-Parra, J.A. Matutes-Aquino, R.A Ochoa-Gamboa, A. Planes, L. Mañosa, D. González-Alonso, M. Stipcich, R. Romero, D. Rios-Jara, and H. Flores-Zuñiga, Phys. Rev. B **83**, 174109 (2011).
[10] M.S. Lund, J.W. Dong, J. Lu, X.Y. Dong, C.J. Palmstrom, and C. Leighton, Appl. Phys. Lett. **80**, 4798 (2002).
[11] Z. Li, C. Jing, J. Chen, S. Yuan, S. Cao, and J. Zhang, Appl. Phys. Lett. **91**, 112505 (2007).
[12] V. K. Sharma, M.K. Chattopadhyay, and S.B. Roy, Phys. Rev. B **76**, 140401R (2007).
[13] D. Y. Cong, S. Roth, J. Liu, Q. Luo, M. Potschke, C. Hurrich, and L. Schultz, Appl. Phys. Lett. **96**, 112504 (2010).
[14] Y. Wang, C. Huang, H. Wu, J. Gao, S. Yang, D. Wang, X. Ding, X. Song, and X. Ren, Appl. Phys. Lett. **102**, 141909 (2013).
[15] S. Aksoy, T. Krenke, M. Acet, E.F. Wasserman, X. Moya, L. Mañosa, and A. Planes, Appl. Phys. Lett. **91**, 251915 (2007).
[16] F. Albertini, S. Fabbrici, A. Paoluzi, J. Kamarad, Z. Arnold, L. Righi, M. Solzi, G. Porcari, C. Pernechele, D. Serrate, and P. Algarabel, Mat. Sci. Forum, **684**, 151 (2011).
[17] L. Mañosa, X. Moya, A. Planes, O. Gutfleisch, J. Lyubina, M. Barrio, J.L. Tamarit, S. Aksoy, T. Krenke, and M. Acet, Appl. Phys. Lett. **92**, 012515 (2008).
[18] L. Mañosa, D. González-Alonso, A. Planes, E. Bonnot, M. Barrio, J.L. Tamarit, S. Aksoy, and M. Acet, Nature Mater. **9**, 478 (2010).
[19] L. Mañosa, D. González-Alonso, A. Planes, M. Barrio, J.L. Tamarit, I.S. Titov, M. Acet, A. Bhattacharyya, and S. Majumdar, Nature Comm. **2**, 595 (2011).
[20] S. Yüce, M. Barrio, B. Emre, E. Stern-Taulats, A. Planes, J.L. Tamarit, Y. Mudryk, K.A. Gschneidner, V.K. Pecharsky, and L. Mañosa, Appl. Phys. Lett. **101**, 071906 (2012).
[21] B. Emre, S. Yuce, E. Stern-Taulats, A. Planes, S. Fabbrici, F. Albertini, and L. Mañosa, J. Appl Phys. **113**, 213905 (2013).
[22] F. Pérez-Reche, M. Stipcich, E. Vives, L. Mañosa, A. Planes, and M. Morin, Phys. Rev. B **69**, 064101 (2004).
[23] K.A. Gschneidner Jr, V.K. Pecharsky, and A.O. Tsokol, Rep. Prog. Phys. **68**, 1479 (2005).
[24] E. Brück, J. Phys. D: Appl. Phys. **38**, R381 (2005).
[25] L. Mañosa, A. Planes, and M. Acet, J. Mater. Chem. A **1**, 4925 (2013).

Copyright line will be provided by the publisher